The Effect of Specimen Strength and Thickness on Cracking Susceptibility during the Sigmajig Weldability Test

Increasing strength and thickness reduce the threshold stress for solidification cracking in A-286 stainless steel

BY J. C. LIPPOLD, S. S. SHADEMAN AND W. A. BAESLACK III

ABSTRACT. The effects of yield strength and specimen thickness on the threshold stress for solidification cracking using the Sigmajig weldability test have been determined for A-286 stainless steel. An increase in test specimen yield strength results in a decrease in the threshold stress for cracking. This decrease is attributed in part to a decrease in the width of the plastically deformed weld zone as the yield strength increases, which enhances strain localization in this region and promotes solidification cracking. Over a range of yield strengths, an increase in specimen thickness generally results in higher threshold stresses for cracking, which are attributed to an increased inherent restraint. The relationship between weld pool shape, the solidification grain structure and the fracture stress during transverse loading (as experienced during Sigmajig testing) has been investigated by performing hot-ductility tests of weld fusion zone specimens. The hot-ductility behavior of specimens produced from welds exhibiting elliptical and teardrop-shaped weld pools is comparable. However, specimens produced from welds that exhibit a teardrop-shaped weld pool fracture along the fusion zone centerline above the nil-ductility temperature, whereas specimens produced from welds that exhibit an elliptical-shaped weld pool fracture in the partially melted zone. A correlation was observed between the fracture stress measured by hot-ductility testing and threshold stresses measured using the Sigmajig test.

J. C. LIPPOLD, S. S. SHADEMAN and W. A. BAESLACK III are with The Ohio State University, Columbus, Ohio.

Introduction

Weld solidification cracking has been a persistent problem in a variety of engineering alloys. Despite numerous studies of this phenomenon, the precise mechanisms responsible for cracking are not completely understood, and the accurate prediction of cracking susceptibility using a purely theoretical approach is not possible. As a result, a large number of weldability test techniques have been developed in an attempt to quantify susceptibility to weld solidification and liquation-related cracking. A recent review of the welding literature revealed that over 150 separate and distinct tests to evaluate these cracking phenomena have been devised over the past 50 years (Ref. 1).

Despite the large number of available weldability test techniques, only a few are applicable to thin-gauge material, particularly in thicknesses less than 3 mm (0.12 in.). The majority of thin-sheet weldability tests are of the representative, or self-restraint, type. Relative to the simulative, or augmented stress/strain type tests, the representative tests provide only a qualitative measure of cracking susceptibility. Recognizing this deficiency for evaluating sheet materials, Goodwin (Ref. 2) developed the Sigmajig test in 1986.

KEY WORDS

Sigmajig Test
Weldability
Weldability Test
Strength
Thickness
Crack Susceptibility
Threshold Stress
A-286 Stainless Steel
Gleeble Test
Hot-Ductility Test
Fracture Morphology

The Sigmajig test is capable of imposing a fixed, uniaxial stress (hence the "sigma") on small sheet samples while an autogenous, full-penetration weld is performed perpendicular to the stress direction. By sequentially increasing the stress level until cracking occurs, a "threshold stress" for solidification cracking can be determined. The threshold stress has been shown to correlate very well with cracking susceptibility for a number of thin-gauge engineering alloys (Ref. 2). In general, the development of comparative weldability indexes using the Sigmajig test has been restricted to materials of similar thickness and strength levels. As a result, there is some question as to its applicability when comparing materials of significantly different thickness and/or strength levelS since both these variables may influence the distribution of stress in the weld region during testing, and therefore, the propensity for solidification cracking.

In response to this uncertainty, the present study was devised to evaluate both specimen thickness and base metal strength effects on Sigmajig test results. In order to accomplish this without introducing additional metallurgical variables, it was deemed necessary to select a single alloy whose strength could be altered over a large range via thermome-

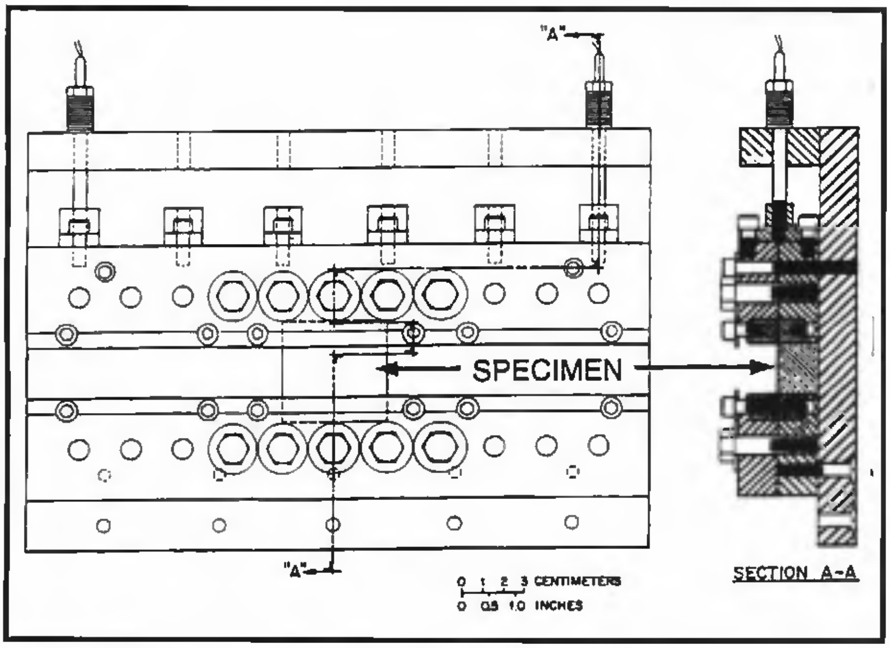

Fig. 1 — Schematic of Sigmajig apparatus.

chanical processing and heat treatment. An additional requirement was that the material be relatively susceptible to weld solidification cracking. To satisfy these requirements, Alloy A-286, a fully austenitic, age-hardenable stainless steel was selected for this investigation.

It is well known that weld pool shape (*i.e.*, elliptical vs. teardrop) can markedly influence solidification cracking susceptibility (Ref. 4). In order to study the influence of weld pool shape and the resulting grain morphology on Sigmajig test results, Gleeble hot-ductility testing was performed on A-286 weld specimens. The effect of the fusion zone grain morphology as influenced by weld pool shape on the hot strength and ductility were determined for comparison with results obtained from Sigmajig testing.

The Sigmajig Test

In the mid-1960s, the Varestraint test was developed, and it is still widely used for the evaluation of weld solidification cracking (Ref. 3). Although this test is sensitive to factors affecting solidification,

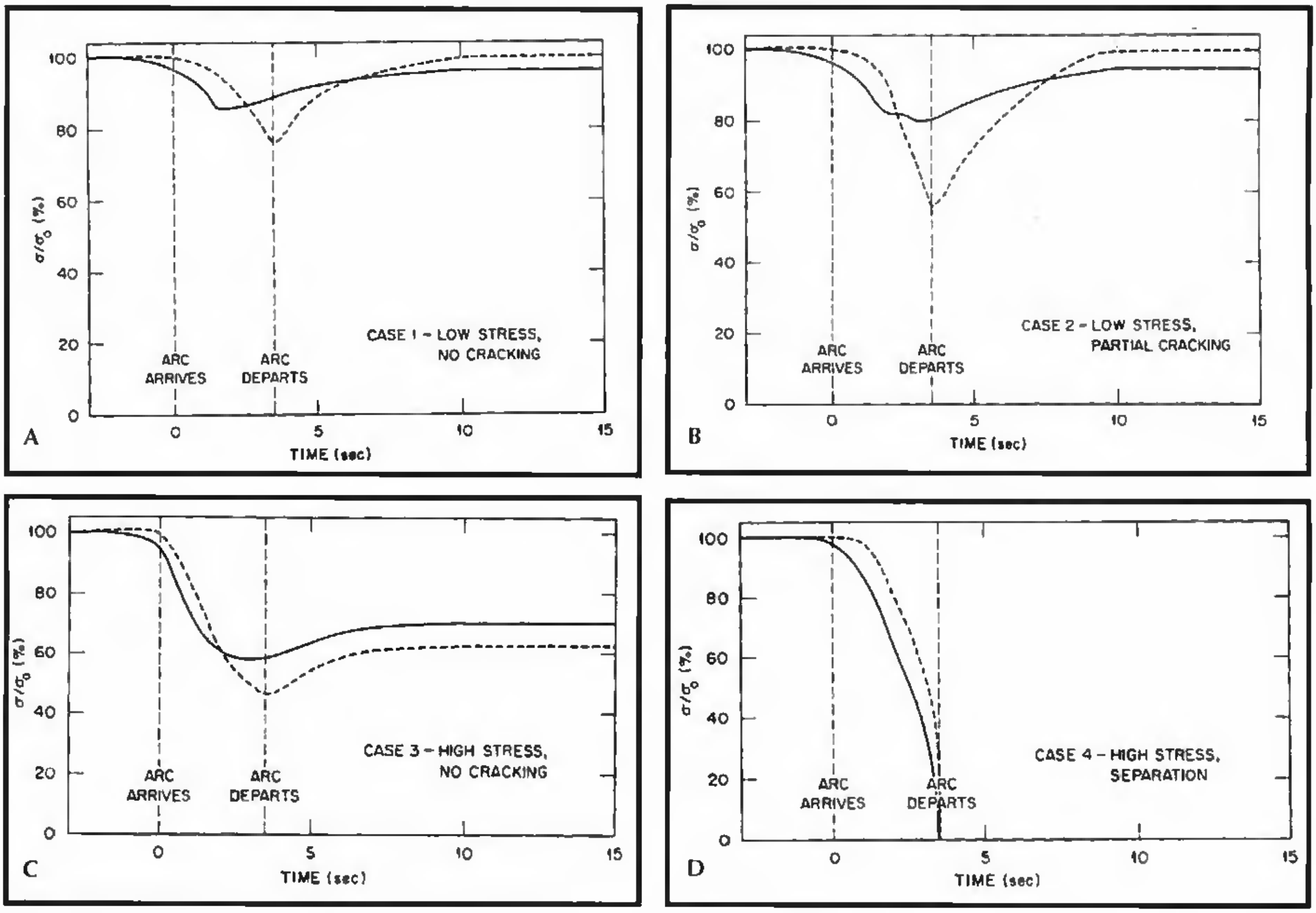

Fig. 2 — Normalized stress vs. time during Sigmajig testing. A — Low stress/no cracking; B — low stress/partial cracking; C — high stress/no cracking; D — high stress/complete specimen separation (from Ref. 2).

such as heat-to-heat variation in composition and impurity level, it is not generally practical for material less than 3 mm in thickness. The Sigmajig test, developed by Goodwin (Ref. 2), can be used to evaluate weld solidification cracking in material down to 0.25 mm (0.01 in.) in thickness. This test is accurate, economical, reproducible, and is also sensitive to factors affecting solidification cracking. The Sigmajig test, like the Varestraint test, is a simulative test technique rather than a representative test in which strain arises from the self-imposed restraint of the system.

The Sigmajig test assembly, with a test specimen in place, is shown in Fig. 1. The fixture holds a 2 x 2-in. (approximately 50 x 50-mm) specimen between hardened steel grips and applies a predetermined initial stress prior to welding. The load is applied through a pair of strain-gauged bolts and maintained by stacks of Bellville washers in the load train. The washers provide an adjustable spring constant. Preliminary testing is generally performed under no-stress conditions to determine autogenous GTA welding parameters, which provide a full-penetration, teardrop-shaped weld pool. During the test program for a given material, the stress is increased sequentially on progressive specimens until a level is reached where centerline cracking initiates at the trailing edge of the weld pool.

The dynamic response of the load cell during testing is shown in Fig. 2 (Ref. 2). The solid curves represent the normalized stress measured by the load cell on the starting side of the specimen (left side in Fig. 1), while the dashed curves represent the normalized stress measured by the load cell on the finishing side (right side in Fig. 1). Figure 2A shows the stress curves for a specimen tested at low stress which experiences no cracking. Stress measured by the first load cell increases as the arc approaches, reaches a minimum when the arc is approximately halfway along the specimen length, and then recovers to essentially the starting level as the specimen cools. The second load cell responds later than the first, with the stress reaching a minimum and then recovering similarly. At low stress with partial cracking (Fig. 2B), the first load cell shows the onset of cracking as a secondary dip on the stress curve after the initial minimum stress has been reached. At high stress with no cracking (Fig. 2C), considerable yielding occurs and the stresses recover to only a fraction of their initial value. In the case of 100% cracking (Fig. 2D), both stress levels monotonically decrease to zero as specimen separation occurs.

In the Sigmajig test, the relative susceptibility to weld solidification cracking is evaluated by the threshold stress, sigma$_{th}$ (σ_{th}). This is defined as the minimum amount of stress that promotes a centerline crack. As the applied stress (sigma) increases, the crack length increases until a point is reached where complete sample separation occurs. The cracking data can fall into two categories as shown in Fig. 3 (Ref. 2). This figure plots percent cracking as the fraction of specimen cracked vs. the applied stress. The more susceptible material falls in the first category where cracking occurs at lower stress levels (low σ_{th}) and experiences a gradual transition to 100% cracking or specimen separation. The second category represents a crack-resistant material where solidification cracking or mechanical fracture occurs at higher stress levels (high σ_{th}) and is associated with an abrupt transition to 100% cracking.

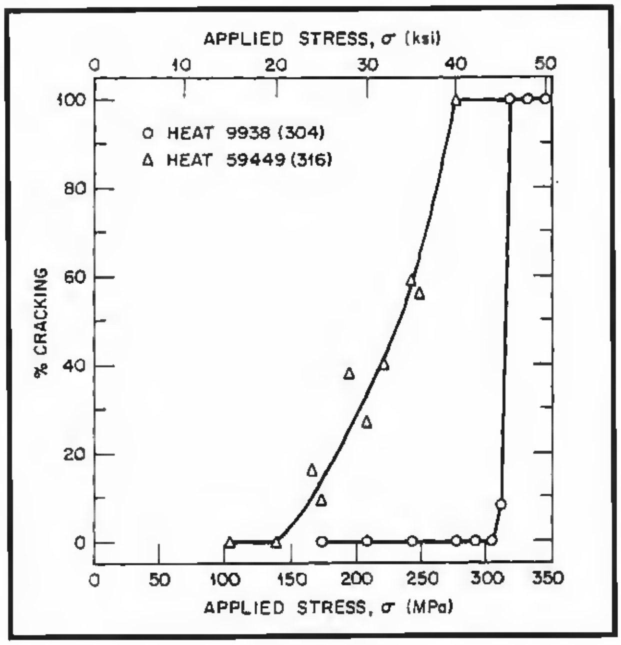

Fig. 3 — Percent cracking vs. applied stress for solidification cracking susceptible and resistant alloys (Ref. 2). The curve to the left represents the more susceptible material.

The Sigmajig test, if utilized properly, can be an effective tool to both discriminate and rank susceptibility to weld metal solidification cracking due to alloy-to-alloy and heat-to-heat variations in composition. Goodwin (Ref. 3), in an investigation of weld metal solidification cracking susceptibility in 0.25-mm (0.1-in.)-thick Type 304 and Type 316 stainless steels, showed a strong effect of alloy chemical composition and primary solidification mode on cracking susceptibility. Consistent with these quantitative results, metallographic analysis of tested specimens with high σ_{th} revealed tensile failure with a large reduction of area. This type of behavior is associated with the sharp transition in percent cracking shown in Fig. 3. Type 316 heats that solidified as primary austenite exhibited appreciably lower threshold stress levels and a gradual transition from 0 to 100% cracking, indicative of a higher susceptibility to solidification cracking.

Results of Sigmajig testing performed by Goodwin and others (Ref. 5) on stainless steels and a variety of other alloys (Fig. 4) indicate that the Sigmajig test can be used as an effective tool to determine the susceptibility of thin sheet material to solidification cracking. The Sigmajig test was shown to be highly responsive to changes such as heat-to-heat variations in composition and impurity levels, weld

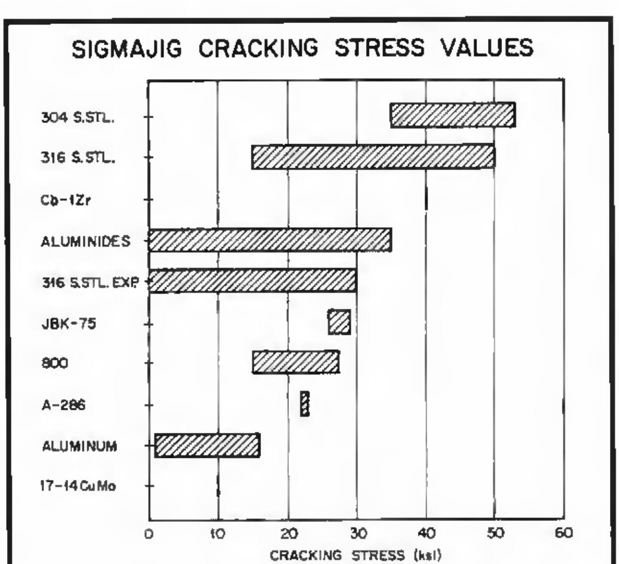

Fig. 4 — Sigmajig threshold stress levels for various alloys (Ref. 4).

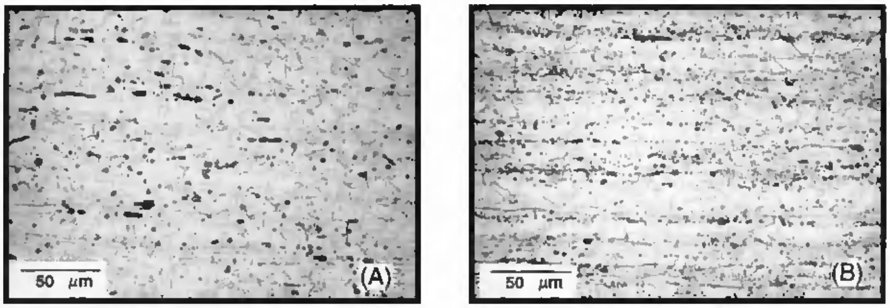

Fig. 5 — Base metal microstructures of A-286 sheet. A — 0.032-in.-thick sheet; B — 0.125-in.-thick sheet (400X).

pool shape, heat input, and welding process (Refs. 2, 5). However, for a given material, the effect of variations in specimen thickness and base metal yield strength on the quantitative weldability test data obtained from the Sigmajig test has not been determined. These are important variables since their differences can strongly influence the distribution of stress at the trailing edge of the weld pool and correspondingly affect solidification cracking susceptibility.

Hot-Ductility Testing

The loss of ductility in the heat-affected zone (HAZ) of a single-pass weld, and previously deposited weld metal in a multipass weld, has been associated with the onset of grain boundary liquation in these regions. The Gleeble hot-ductility test was developed to synthetically reproduce thermal cycles similar to those experienced in the actual weld HAZ so that alloys susceptible to HAZ liquation cracking could be differentiated by their hot-ductility response.

The interpretation of hot-ductility test results has typically been based on the reduction of area (ductility) exhibited by specimens fractured at various temperatures during both the on-heating and on-cooling portions of a simulated weld thermal cycle. This reduction in area is determined by applying a tensile load to fracture the specimen at a specific temperature during either of the two portions of the thermal cycle.

During the on-heating portion of the test, specimens are fractured at increasingly higher temperatures until the nil-ductility temperature (NDT) and the nil-strength temperature (NST) are determined. The NDT corresponds to that temperature where the reduction in area is zero. Although at this temperature the specimen does not exhibit any ductility, it still exhibits some strength. At the NST, the specimen will not exhibit ductility or strength. This is attributed to the extensive liquation of the grain boundaries at this temperature.

During the on-cooling portion of the test, the specimens are fractured at successively lower temperatures after being heated to a peak temperature between the NDT and the NST. This is continued beyond the ductility recovery temperature (DRT) where a selected level of the ductility is recovered. A material with a low DRT and a slower rate of ductility recovery is considered to be susceptible to HAZ liquation cracking.

Recently, work by Lin, *et al.* (Ref. 6), developed a new methodology for predicting HAZ liquation cracking susceptibility using the Gleeble hot-ductility test. This approach effectively measures a thermal crack susceptible (*i.e.*, brittle) region, which is a material-specific parameter and which provides a measure of liquation cracking susceptibility.

Although Gleeble hot-ductility testing is used principally to characterize susceptibility to weld HAZ liquation cracking, recent work by Chen (Ref. 7) has shown that the testing of weld fusion zone specimens can provide useful information regarding the nature of solidification cracking. This is particularly applicable in materials where diffusivity is low (such as FCC materials) and significant microstructural variation does not occur upon reheating in the Gleeble.

In the present investigation, Gleeble hot-ductility testing of weld metal specimens was performed specifically to study the effects of weld pool shape and the resulting solidification-induced grain structure on the nature of solidification cracking as experimentally determined using the Sigmajig test.

Table 1 — Chemical Composition of A-286 Sheet Material (wt-%)

	Sheet thickness	
Element	0.125 in. (3.17 mm)	0.062 in. (1.57 mm)
C	0.067	0.057
Mn	0.161	0.164
P	0.026	0.028
S	0.011	0.011
Si	0.159	0.206
Ni	24.40	24.27
Cr	14.50	14.47
Mo	1.25	1.27
Cu	0.180	0.182
Al	0.361	0.363
Ti	2.47	2.51
V	0.137	0.134

Objectives

The objectives of this investigation were as follows:

1) Determine the effects of base metal strength and thickness on solidification cracking behavior as measured by the Sigmajig weldability test.

2) Determine possible correlations between Sigmajig testing and Gleeble hot-ductility testing of weld metal specimens.

Experimental Procedure

Materials

Chemical compositions of the two heats of A-286 evaluated in this investigation are listed in Table 1. Sheet material in both 0.125-in. (3.17-mm) and 0.032-in. (0.82-mm) thicknesses were provided in the solution heat-treated condition. Representative microstructures of the as-received base metals, shown in Fig. 5, exhibit a recrystallized austenitic grain structure and a bimodal distribution of titanium carbides and/or carbonitrides. Presumably, the coarse carbides form during casting of the original material while the finer precipitates form during subsequent processing steps.

Thermomechanical Processing

Achieving four tensile strength levels in two specimen thicknesses suitable for Sigmajig testing was accomplished by heat treatment of the 0.032-in. (0.82-mm) sheet and by cold rolling and heat treatment of the 0.125-in. (3.17-mm) sheet. Samples produced from the 0.032-in. sheet were aged at 718°C (1324°F) for 2, 8 and 16 h. Samples of 0.125-in. sheet were cold rolled to a reduction of 50% (~0.062 in., 1.57 mm) and either direct aged at 718°C/4 h or solution heat treated at 900°C (1652°F) for 10 min, and then aged at 718°C for 4 and 16 h. Tensile specimens were machined from the heat-treated sheets (gauge section: 2.0 in. long x 0.4 in. wide/50.8 x 10.2 mm) and tested at an extension rate of 0.05 in./min (0.021 mm/s). Tensile test results under various thermomechanical treatments for both sheet thicknesses are summarized in Table 2.

Table 2 — Material Condition and Corresponding Strength and Hardness as a Function of Thickness

Material Condition	Yield Strength, ksi (MPa)	Ultimate Tensile Strength, ksi(MPa)	Average Hardness (Knoop)
0.032 in. (0.82 mm) thick material			
1 — As-received	55 (379)	91 (627)	167
2 — Condition 1, and aged 2 h at 718°C	94 (648)	157 (1082)	313
3 — Condition 1, and aged 8 h at 718°C	114 (785)	172 (1185)	360
4 — Condition 1, and aged 16 h at 718°C	118 (813)	167 (1151)	392
0.062-in. (1.57-mm) thick material			
5—As-Rolled (50% reduction from 0.125 in.)	138 (951)	146 (1006)	369
6—Condition 5, and aged 4 h at 718°C	177 (1220)	192 (1323)	432
7—Condition 5, and solution annealed at 899°C for 10 min	63 (434)	103 (710)	202
8—Condition 7, and aged 16 h at 718°C	130 (896)	176 (1213)	380

Table 3 — Sigmajig Test Welding Conditions

	0.032-in. (0.82-mm) sheet	0.062-in. (1.57-mm) sheet
Welding Process	GTAW (DCEN)	GTAW (DCEN)
Current	70 A	110 A
Voltage	10 V	12 V
Travel speed	24 in./min (10.2 mm/s)	24 in./min (10.2 mm/s)
Electrode	W-ThO_2, 1.6-mm diameter, 60-deg included angle	W-ThO_2, 1.6-mm diameter, 60-deg included angle
Electrode/work distance	0.035 in. (0.89 mm)	0.035 in. (0.89 mm)
Shielding gas	Argon, 15 cfh (7 L/min)	Argon, 15 cfh (7 L/min)
Heat input	1.75 kJ/in. (0.07 kJ/mm)	3.3 kJ/in. (0.13 kJ/mm)
Average weld width	0.129 in. (3.28 mm)	0.165 in. (4.19 mm)

Table 4 — Welding Conditions for Preparation of Gleeble Hot-Ductility Samples

	Elliptical Pool Shape	Teardrop Pool Shape
Welding Process	GTAW (DCEN)	GTAW (DCEN)
Current	70 A	170 A
Voltage	18 V	19.5 V
Travel speed	6 in./min (2.54 mm/s)	20 in./min (8.5 mm/s)
Electrode	W-ThO_2, 3.1-mm diameter, 60-deg included angle	W-ThO_2, 3.1-mm diameter, 60–deg included angle
Electrode/work distance	3 mm (0.12 in.)	3 mm (0.12 in.)
Shielding gas	Helium, 50 cfh (23.5 L/min)	Helium, 50 cfh (23.5 L/min)
Heat input	12.6 kJ/in. (0.5 kJ/mm)	9.94 kJ/in. (0.4 kJ/mm)
Average weld width	0.195 in. (4.96 mm)	0.225 in. (5.72 mm)

Sigmajig Testing

Sigmajig test specimens were sheared to 2 x 2-in. (50 x 50-mm) dimensions from material that was thermomechanically processed and/or heat treated to provide eight thickness/strength combinations. Twenty samples were prepared for each thickness/strength condition. Heat-treated specimens were grit-blasted to remove scale. All samples were cleaned with acetone immediately prior to testing. Before actual testing, several specimens of each thickness were welded under no load in the Sigmajig fixture in order to determine welding parameters that provide a full-penetration weld with a teardrop-shaped weld pool. The GTA welding parameters utilized for both sheet thicknesses are provided in Table 3.

Applied stresses starting from 12 ksi (82.6 MPa) were increased sequentially by 3 ksi (20.5 MPa) on each progressive specimen until centerline crack initiation occurred. Then the applied stress was reduced by 0.5 ksi (3.4 MPa) and the test was repeated. If crack initiation again occurred, the applied stress was reduced by the same increment and testing repeated. If there was no crack initiation, the previous higher applied stress was determined to be the threshold stress for cracking. In all cases, the threshold stress was determined as the applied stress required to promote any cracking in the samples. This procedure is consistent with that recommended by Goodwin (Refs. 2, 4).

Hot-Ductility Testing

Full-penetration, autogenous GTA welds exhibiting either an elliptical- or teardrop-shaped weld pool were produced on the 0.125-in. (3.17-mm) thick sheet using the welding parameters given in Table 4. The welding direction was normal to the sheet rolling direction. Hot-ductility specimens were machined to dimensions of 0.5 x 4.0 in. (12.7 x 101.6 mm), with the weld fusion zone centerline located at the center of the 4.0-in. dimension. The jaw spacing was maintained at 0.75 in. (19 mm) throughout the test program.

For the on-heating portion of the hot ductility test, the Gleeble was programmed to reach the selected peak temperatures at a rate of 93.3°C/s (168°F/s). After the peak temperature was reached, the current was shut off, and the sample was immediately fractured at a rate of 50 mm/s. NDT and NST temperatures were determined using previously developed practices (Ref. 6).

For the on-cooling part of the hot-ductility test, samples were heated at a rate of 93.3°C/s to a peak temperature 25°C (45°F) below the NST, and cooled at a rate of 45°C/s (81°F/s) prior to their fracture at 25°C intervals. The fracture area dimensions were measured by a binocular microscope equipped with a calibrated eyepiece.

Metallurgical Characterization

Metallographic samples were removed from both the Sigmajig and Gleeble hot-ductility test specimens. Specimens were mounted in bakelite, polished through 0.06-micron colloidal silica and etched electrolytically in 10% oxalic acid solution at a voltage of 6 V. Specimen fracture surfaces for examination in the scanning electron microscope (SEM) were also prepared from Sigmajig and Gleeble hot-ductility test specimens. The cracked Sigmajig samples were opened by carefully cutting perpendicular to both crack tips and breaking the section apart.

Results

The final selection of thermomechanical processing and/or heat treatments which provided materials of two different

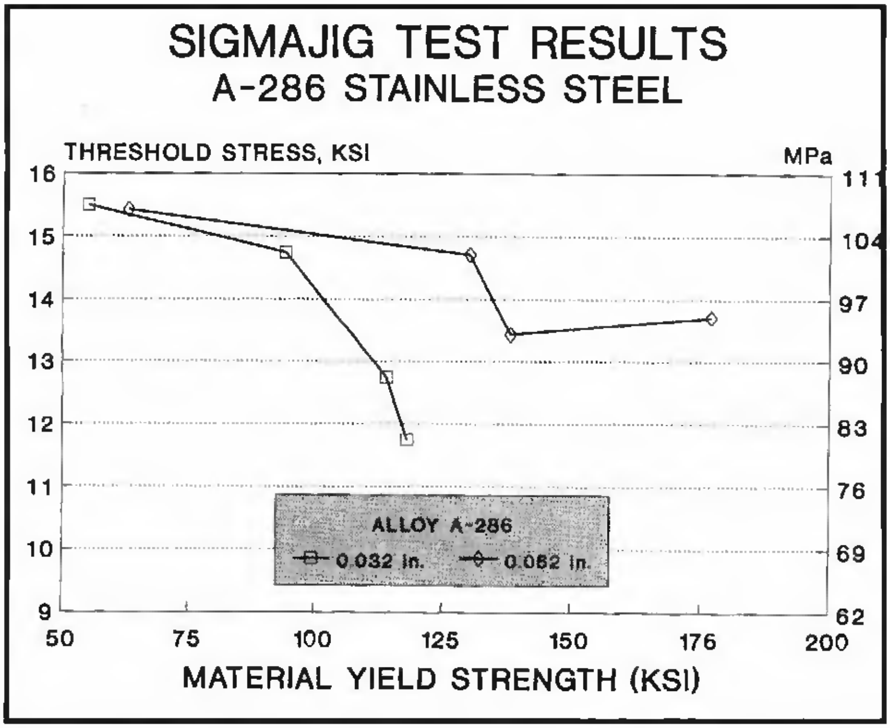

Fig. 6 — Threshold stress vs. specimen yield strength for 0.032- and 0.062-in.-thick sheet.

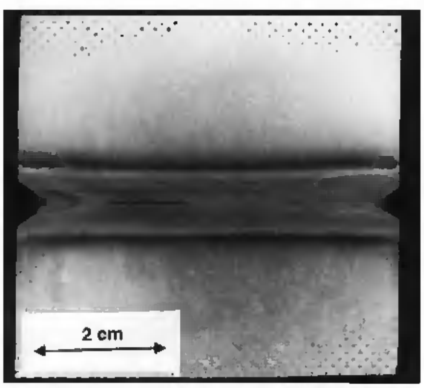

Fig. 7 — As-tested Sigmajig test specimen of 0.032-in.-thick sheet.

thicknesses and four different strength levels was initially based on hardness measurements. Table 2 summarizes the material conditions and their corresponding yield strengths (determined by tensile testing) selected from the 0.032-in. (0.82-mm) annealed sheet and 0.062-in. (1.58-mm) cold-rolled and annealed sheet. As shown, although a range of strengths was achieved for the two thicknesses, it was not possible to precisely match yield and tensile strengths for the same thermomechanical conditions.

Sigmajig Test Results

Sigmajig test results in terms of threshold stress to cause cracking vs. base metal yield strength are presented in Fig. 6. Note that for both material thicknesses, increasing base metal yield strength resulted in a decrease in the σ_{th} (the minimum stress required to cause solidification cracking). This effect was most pronounced in the thinner material. Figure 6 also shows that decreasing specimen thickness resulted in a decrease in σ_{th} particularly at high base metal yield strength values.

Figure 7 shows a cracked Sigmajig test specimen produced from the as-received 0.032-in. material tested at 17.5 ksi (120.6 MPa). Figure 8A and B shows plan and transverse section views, respectively, of the cracked specimen in Fig. 7. The centerline solidification crack has initiated and propagated at the solidification grain boundary produced between impinging columnar grains at the weld centerline of the teardrop-shaped weld pool. The fusion zone microstructure consists of a fully austenitic, cellular dendritic solidification morphology and was essentially identical for both sheet thicknesses.

A number of fracture surfaces were examined in the SEM in order to verify the mechanism of crack formation in the A-286 material during Sigmajig testing. Figure 9A is a macrograph of the fracture surface of a test specimen of as-rolled 0.062-in. (1.58-mm) thick material (YS = 138 ksi/951 Mpa) tested at 15 ksi (103.3 MPa). High-magnification fractographs at selected locations in this figure are shown in Fig. 98–D (Location 1 indicates the crack initiation region, Location 3 indicates the crack arrest region). All surfaces exhibit dendritic features with negligible evidence of solid-state (ductile-rupture) fracture. Locations 2 and 3 exhibit noticeably coarser dendritic features than Location 1, with evidence of secondary dendrite arms.

Hot-Ductility Testing

The hot-ductility behavior of welded specimens produced with teardrop- and elliptical-shaped weld pools are shown

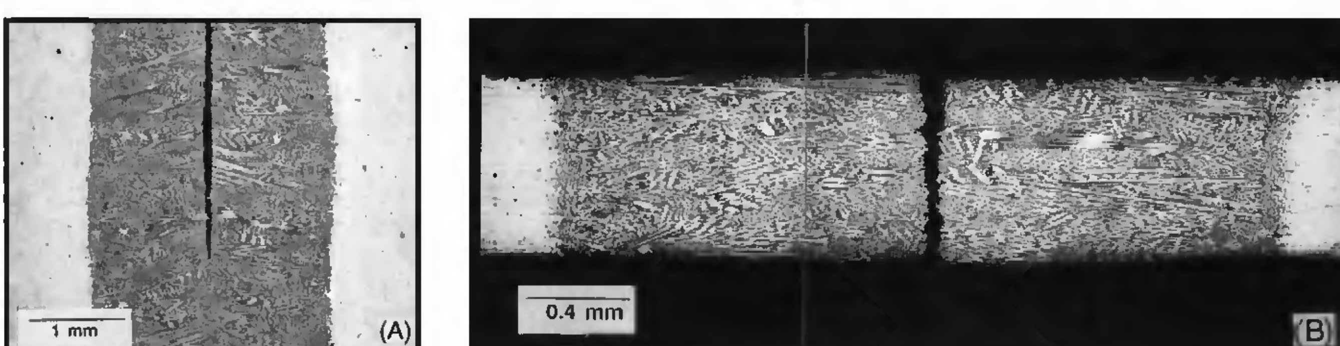

Fig. 8 — Views of cracked Sigmajig test specimen of 0.032-in.-thick sheet (see Fig. 7). A — Plan view, 25X; B — transverse view, 50X.

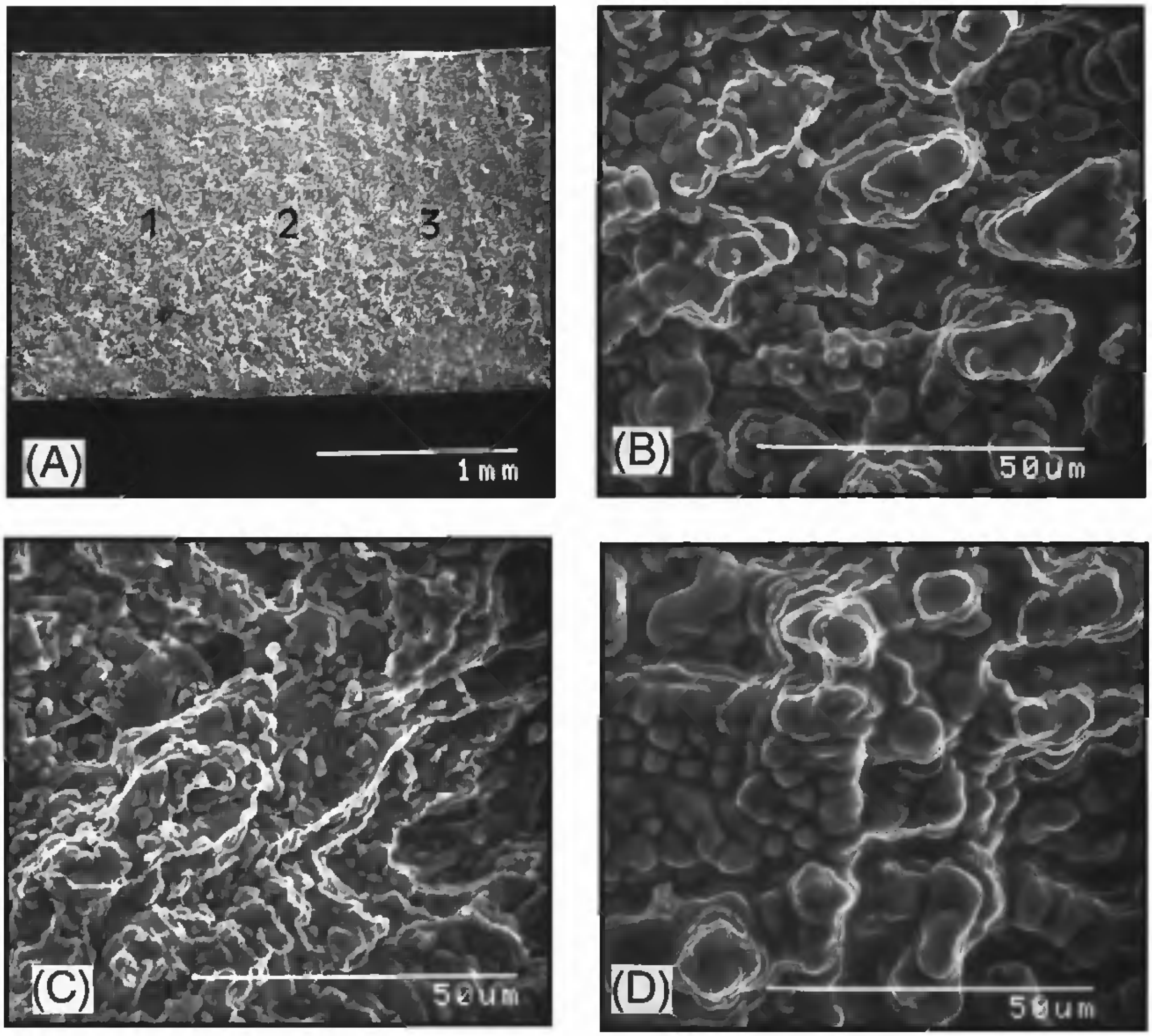

Fig. 9 — SEM fractograph of cracked Sigmajig sample. A — 30X; B–D — Locations 1–3 in A, 1000X.

in Figs. 10 and 11. Both on-heating and on-cooling data indicate that weld pool shape has a negligible effect on the NDT, NST and DRT of the A-286 material. Consequently, the on-cooling nil-ductility range (T_p-DRT_{Tp}), which is a measure of the materials susceptibility to liquation cracking, appears to be independent of the weld pool shape and its microstructural characteristics. Figure 11 shows plots of fracture stress vs. temperature for the two weld pool types. Again, weld pool morphology shows little relationship to on-heating or on-cooling fracture stress.

Fracture location in the hot-ductility specimens was found to be dependent on weld pool shape. For the teardrop-shaped weld pool specimens, the fracture site shifted from the HAZ to the fusion zone centerline at a temperature about 75°C (135°F) above the NDT. Fracture of specimens produced from elliptical-shaped weld pools occurred exclusively within the HAZ. Figure 12A and B shows a plan view of the welds exhibiting teardrop- and elliptical-shaped weld pools, respectively. Both weld metal microstructures exhibit a cellular-dendritic solidification substructure, with solidification grain boundaries defined by the intersection of dendrites of different orientation. Despite the generation of an elliptical-shaped weld pool at a velocity of 6.0 in./min (2.5 mm/s), both fusion zone macrostructures exhibited a distinct centerline grain boundary. Consistent with the difference in travel speed, however, the weld structure generated from the elliptical pool showed a greater change in solidification direction from the weld interface to the weld centerline.

Figure 13 shows the weld interface region characteristic of welds made using either pool shape. Constitutional liquation of the titanium carbides and appreciable grain boundary liquation were apparent in both welds. During hot-ductility testing, heating to the NDT resulted in negligible change in the weld fusion zone and HAZ microstructures. Heating to the NST temperature, however, resulted in dissolution and spherodization of the interdendritic eutectic constituent in both the fusion zone and HAZ, and promoted increased grain boundary liquation in the HAZ.

Discussion of Results

Sigmajig Test Results

The Sigmajig test results presented in Fig. 6 indicate that σ_{th} for solidification cracking decreases as the base metal yield strength increases. This effect is par-

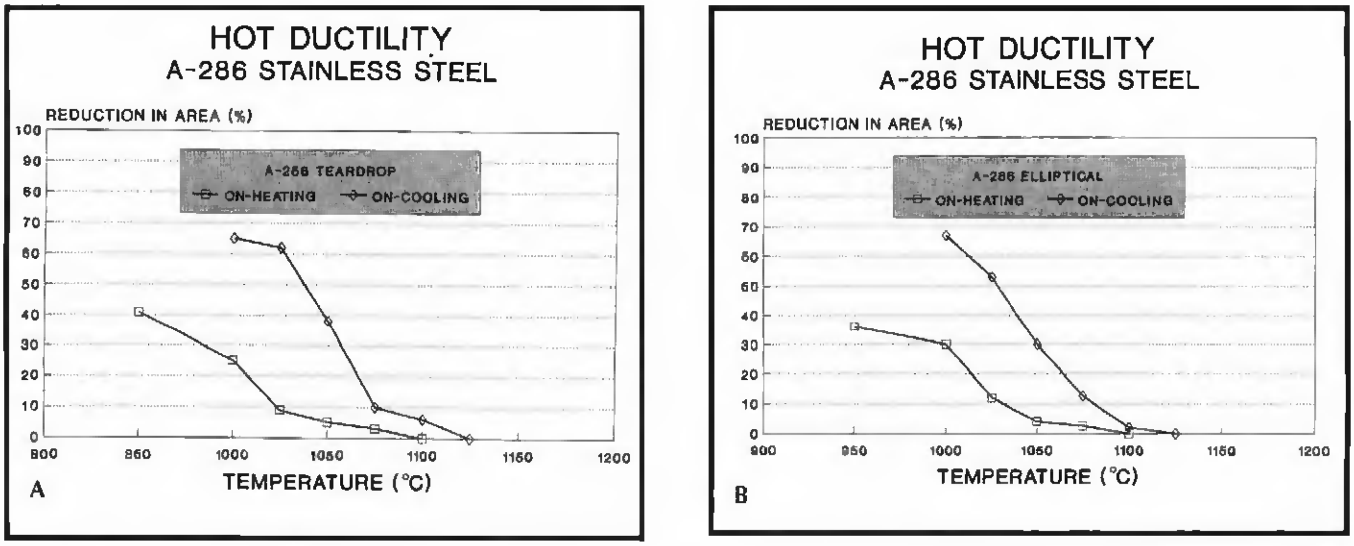

Fig. 10 — Gleeble hot-ductility data for weld metal specimens. A — Teardrop-shaped weld pool; B — elliptical-shaped weld pool.

ticularly pronounced in the 0.032-in. (0.82-mm) thick material. Weld metal solidification cracking during Sigmajig testing results from the contribution of both metallurgical and mechanical factors. Metallurgical factors include the magnitude of the BTR, the ductility within this temperature range, and the amount and wetting characteristics of the terminal liquid present along solidification grain boundaries. These factors are strongly related to material composition and, to a lesser extent, the welding process parameters. The chemical compositions of the as-received materials used in this investigation were essentially identical (Table 1) and the specific welding parameters used for each thickness group were maintained constant during testing. Correspondingly, the microstructural characteristics of welds produced in each respective sheet thickness appeared essentially identical for all yield strength levels.

Based on these metallurgical similarities, it can be concluded that mechanical factors such as thermally induced strain, applied strain and geometric constraint effects are the most important contributors to the observed differences in σ_{th} with specimen yield strength and thickness.

As mentioned earlier, Sigmajig testing consists of two steps. First, a predetermined stress is applied to the specimen. Secondly, a full-penetration autogenous weld bead with teardrop morphology is deposited on the specimen transverse to the applied stress. If centerline cracking is not observed, the applied stress is increased sequentially on progressive specimens until a level is reached where cracking initiates at the trailing edge of the weld pool. It should be noted that this level is reached when the applied stress (which is usually within the elastic range at room temperature) is equal to the threshold stress. The corresponding strain is macroscopic and is given by:

$$\varepsilon_{th} = \frac{\sigma_{th}}{E} = \frac{\Delta L}{W} \qquad (1)$$

where: ε_{th} = threshold strain for cracking; σ_{th} = threshold stress for cracking; E = modulus of elasticity; ΔL = total amount of sample displacement (macroscopic); W = specimen width (2 in.).

Goodwin (Ref. 2) illustrated that the

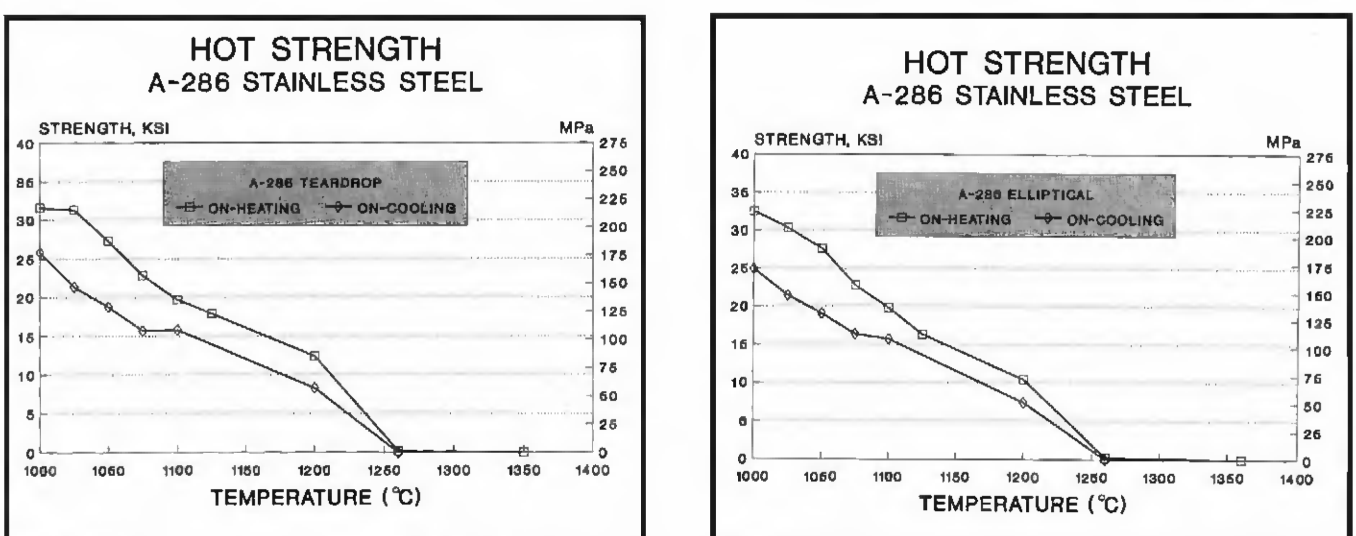

Fig. 11 — Fracture stress vs. temperature for Gleeble weld metal specimens. A — Teardrop-shaped weld pool; B — elliptical-shaped weld pool.

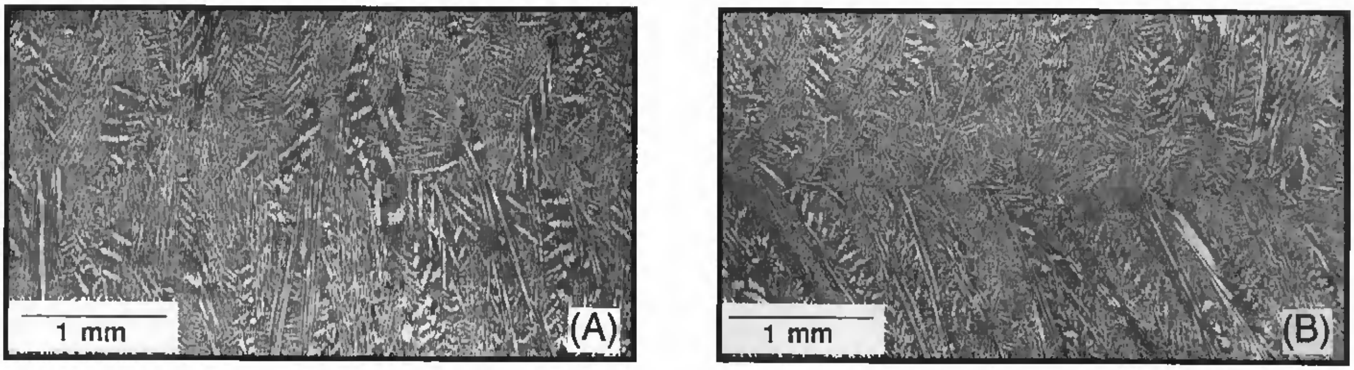

Fig. 12 — Plan views of autogenous GTA welds produced in 0.062-in.-thick sheet. A — Teardrop-shaped weld pool; B — elliptical-shaped weld pool. Arrows indicate weld centerline (25X).

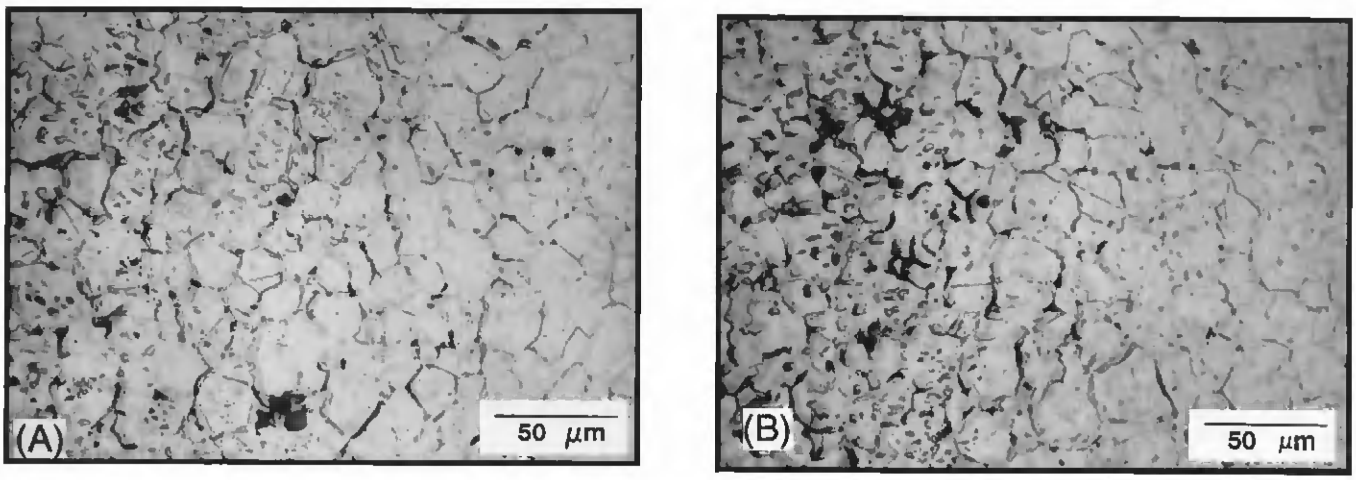

Fig. 13 — Plan views showing the weld interface region of GTA welds produced in 0.062-in.-thick sheet. A — Teardrop-shaped weld pool; B — elliptical-shaped weld pool. Note liquation along grain boundaries (400X).

local applied load (hence the applied stress) decreases during the welding portion of the Sigmajig testing — Fig. 2. Since cracking in the Sigmajig samples occurs at elevated temperatures where the strength of the material is drastically reduced, the applied stress (which in this case is equal to the threshold stress at room temperature) decreases during weld bead deposition. This reduction in applied stress allows the applied strain to be locally concentrated within the plastically deformed region that includes the fusion zone and the near HAZ. Within this region, if the localized strain is greater or equal to a critical localized strain for cracking, solidification cracking will occur. Both localized strains are microscopic and their magnitudes are given by:

$$\varepsilon_{L_o} = \frac{\Delta L}{L_p} \tag{2}$$

$$\varepsilon_c = \frac{\Delta L_c}{L_p} \tag{3}$$

where: ε_{Lo} = localized strain; ε_c = critical localized strain; ΔL = total amount of sample displacement (macroscopic, which is localized in the fusion zone and HAZ during welding); L_p = width of the plastically yielded zone, which includes the fusion zone and HAZ (microscopic); ΔL_c = critical amount of sample displacement to cause cracking.

Using this approach, it can be seen that a reduction in the plastically yielded zone, L_p, increases the magnitude of the localized strain if it is assumed that (ΔL), the total amount of displacement (which during welding is localized in the fusion zone and HAZ), remains constant for all specimens of the same thickness. For fixed welding conditions, the width of the plastically yielded zone can be expected to decrease as the yield strength increases. This effectively reduces the threshold stress necessary to cause cracking. This argument is consistent with the Sigmajig results presented in Fig. 6.

In order to substantiate this theory, microhardness surveys were obtained for both the 0.032-in. (0.82-mm) and 0.062-in. (1.58-mm) Sigmajig samples as shown in Figs. 14 and 15, respectively. Note that as the yield strength of the test specimen increases, the width of the softened region (which includes the fusion zone and HAZ) decreases. This is illustrated schematically in Fig. 16 for specimens of different yield strength under an applied stress.

The relationship between σ_{th} and the width of the fusion zone and softened HAZ can also be determined using the following equation expressing the total displacement (ΔL) of the sample both prior to and during testing, where

$$\underset{\text{prior}}{\Delta L = W \times \sigma/E} = \underset{\text{during testing}}{L_p \times \varepsilon\ (\text{plastic}) + L_e \times \sigma/E\ (\text{elastic})} \tag{4}$$

where, W = sample width = $L_e + L_p$; L_e = width of elastically deformed region of sample; L_p = width of plastically deformed region of sample; ε = amount of plastic strain prior to cracking; E = elastic modulus; σ = pre-applied stress

The elastic strain is negligible during Sigmajig testing since essentially all deformation occurs plastically in the fusion

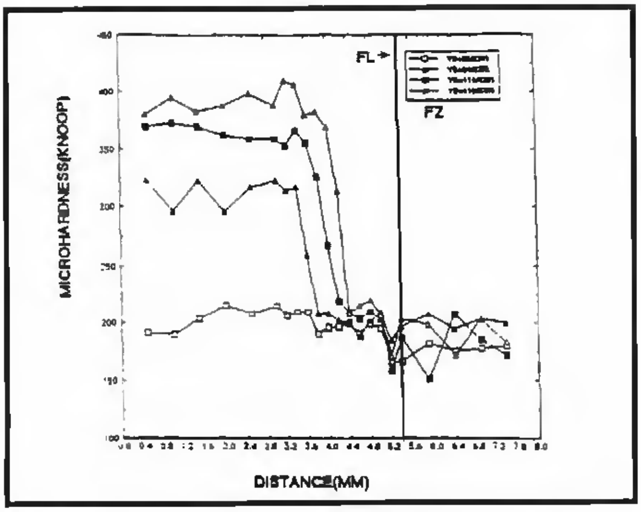

Fig. 14 — Microhardness traverses across the HAZ and fusion zone of Sigmajig test specimens in 0.032-in.-thick sheet at different yield strength levels.

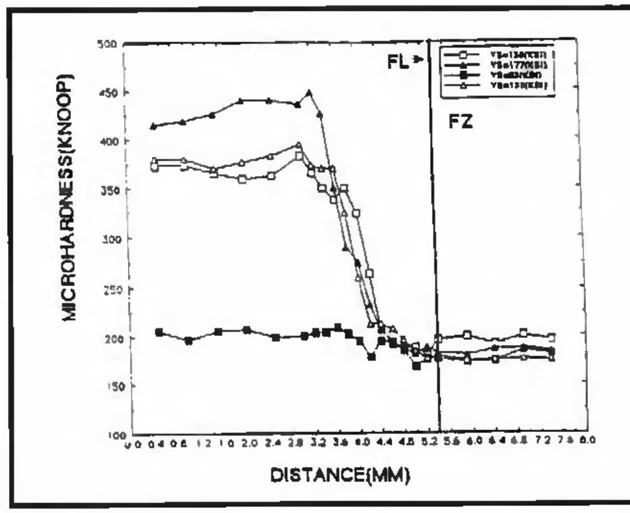

Fig. 15 — Microhardness traverses across the HAZ and fusion zone of Sigmajig test specimens in 0.062-in.-thick sheet at different yield strength levels.

zone and softened HAZ. As a consequence, Equation 4 can be reduced to

$$W \times \sigma/E = L_p \times \varepsilon \qquad (5)$$

When comparing high- and low-strength samples, it can be further assumed that L, E and ε are equivalent and the following relationship derived.

$$\sigma_{th}/\sigma_{thA} = L_p/L_{pA} \qquad (6)$$

where σ_{th} = threshold stress for cracking; σ_{thA} = threshold stress for cracking in annealed sample; L_{pA} = width of fusion zone and softened HAZ region in annealed sample.

These ratios are compared in Table 5 for both the 0.032- and 0.062-in.-thick samples. Note that agreement between these ratios is very good, reinforcing the previous argument relating σ_{th} to the width of the combined fusion zone plus softened HAZ region as influenced by initial base material strength.

Another purpose of this investigation was to observe the effect of varying specimen thickness at equivalent yield strength on the threshold stress. Table 2 showed the material conditions, annealed (Nos. 1 and 7) and aged (Nos. 4 and 8) from the two different thickness materials obtained for this purpose. Although the heat treatment conditions for material conditions No. 4 (0.032-in. thick) and No. 8 (0.062-in. thick) should have produced the same yield strengths, actual tensile testing showed some variations. The yield strengths were found to be 118 ksi (813 MPa) and 130 ksi (896 Mpa), respectively. This discrepancy is attributed to factors such as residual cold work and finer grain size that directly influence the yield strength of the 0.062-in.-thick material. On the other hand, Fig. 6 showed that for the material conditions 1 and 7, with strengths of 55 ksi (379 MPa) and 63 ksi (434 MPa), respectively, the threshold stresses were identical (σ_{th} = 15.5 ksi (107 MPa)). This indicated that at low yield strengths variations in thickness had little effect on the σ_{th}. Increasing the equivalent yield strengths for different thickness material shows an increasingly larger difference between σ_{th} as a function of thickness. This suggests that a relationship exists among material yield strength, σ_{th}, and a geometric factor such as the weld width-to-thickness ratio (W/T). It is assumed here that increasing material thickness correspondingly increases the magnitude of the intrinsic constraint for a given weld width. This "constraint effect" becomes more important as the material thickness increases and/or the width of the softened region decreases.

Gleeble Hot-Ductility Testing

Hot-ductility behavior was found to be relatively unaffected by weld pool shape (Fig. 10), but a significant variation in fracture location was observed, espe-

Table 5 — Correlation between Sigma$_{TH}$ and Width of the Fusion Zone and Softened HAZ

Material Yield Strength, ksi (MPa)	σ_{th} ksi (MPa)	L_p, in. (mm) (1)	σ_{th}/σ_{thA} (2)	L_p/L_{pA} (3)
		0.032-in. (0.82-mm) thick material		
55 (379)	15.5 (107)	0.26 (6.5)	1.0	1.0
94 (648)	14.75 (102)	0.24 (6.1)	0.951	0.938
114 (785)	12.75 (88)	0.21 (5.3)	0.823	0.815
118 (813)	11.75 (81)	0.19 (4.9)	0.758	0.754
		0.062-in. (1.57-mm) thick material		
63 (434)	15.5 (107)	0.23 (5.9)	1.0	1.0
130 (896)	14.75 (102)	0.215 (5.5)	0.951	0.932
138 (951)	13.5 (93)	0.20 (5.1)	0.871	0.864
177 (1220)	13.75 (95)	0.205 (5.2)	0.887	0.881

(1) Determined from microhardness traverses in Figs. 14 and 15.
(2) Ratio of critical stress to cause cracking in thermomechanically strengthened samples to annealed samples.
(3) Ratio of width of fusion and softened HAZ in thermomechanically strengthened samples to annealed samples.

cially at temperatures equivalent to or higher than the NST. When weld samples were reheated in the Gleeble, simultaneous liquation occurred in both the fusion zone and HAZ. This liquation is attributed to the presence of a low-melting constituent (Laves phase) along both solidification boundaries in the weld metal and grain boundaries in the HAZ. The extent of liquation depends on the peak temperature. When stress was applied during hot-ductility testing, the liquated regions were separated and fracture occurred either interdendritically (along solidification grain and subgrain boundaries) in the weld metal or intergranularly in the HAZ.

At the NDT temperature, liquation in the fusion zone is inevitable, but appears to be less extensive than that in the HAZ where constitutional liquation has created continuous low-melting networks in the narrow region close to the weld interface. As a result, fracture at the NDT occurs preferentially at grain boundaries in the HAZ. Reheating to temperatures near the NST results in extensive intergranular liquation in both the fusion zone and HAZ. During resolidification upon cooling to the DRT, the grain and subgrain boundaries in the fusion zone are severely embrittled due to the persistence of low-melting liquids. For the teardrop-shaped weld pool, the applied stress on-cooling to the DRT results in strain concentration along the weld centerline since a liquated region is present that is perpendicular to the direction of applied stress. In samples prepared from elliptical pool shapes, a distinct "line" of liquation is not present in the fusion zone and the potential fracture path in the weld metal becomes more tortuous. As a result, fracture occurs preferentially along the heavily liquated HAZ region adjacent to the fusion boundary.

Correlation between Sigmajig and Gleeble Hot-Ductility Testing

Based on hot-ductility testing, the BTR, or temperature regime over which liquid films persist on-cooling, was independent of weld pool shape. Based on recent work by Lin, *et al.* (Refs. 6, 8, 9), the BTR for both weld shapes as defined by the temperature range T_L–DRT_{TL} is approximately 400°C (752°F) with the fracture stress ranging from zero at and above the NST to 19 ksi (131 MPa) at the DRT.

Since weld metal solidification cracking occurs during the cooling portion of the thermal cycle, the cracking index for hot-ductility testing, the T_L–DRT_{TL} (400°C) range, can be related to the temperature range during which weld metal

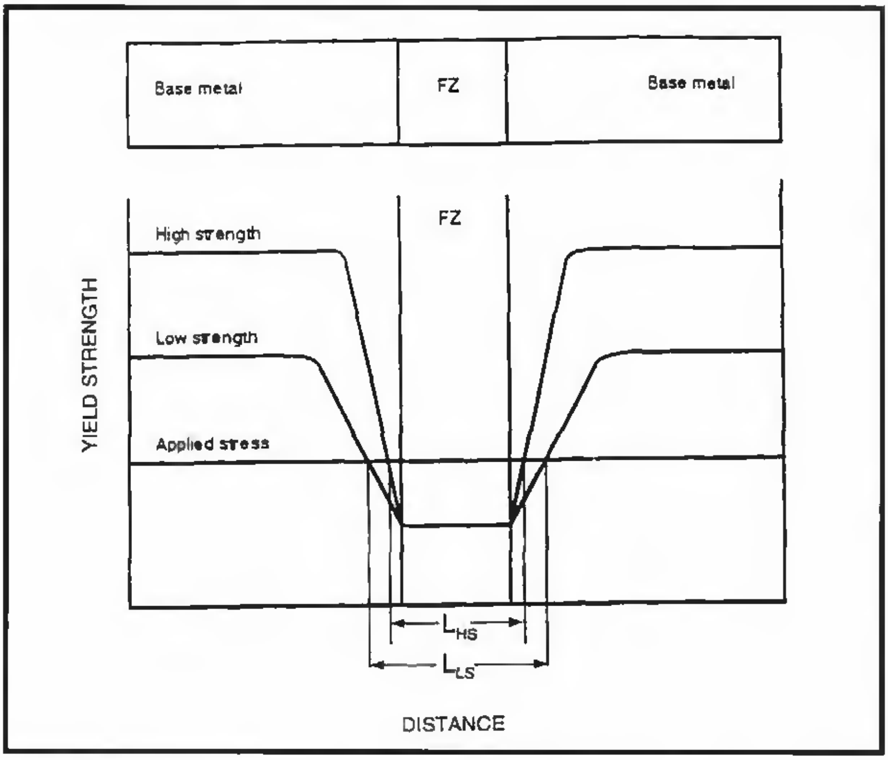

Fig. 16 — Hypothetical yield strength vs. distance across Sigmajig test specimens at two base metal yield strength levels with applied Sigmajig stress level superimposed. The width of the zone which may undergo plastic yielding during testing for each case is indicated by L_{HS} and L_{LS}.

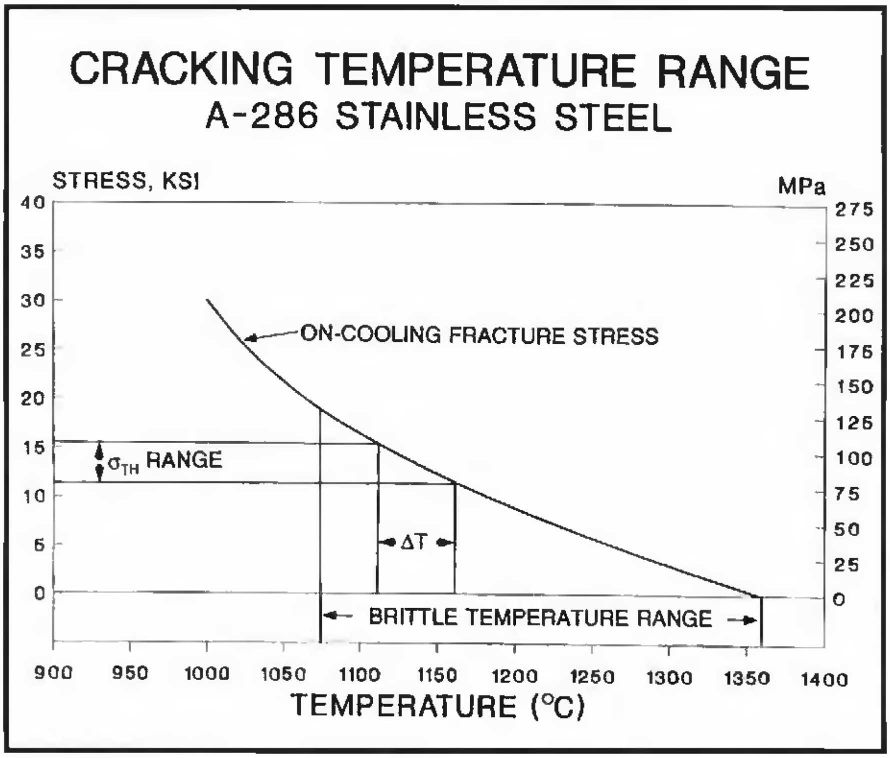

Fig. 17 — Fracture stress vs. temperature for the on-cooling portion of hot-ductility test of a teardrop-shaped weld pool. Sigma$_{th}$ values have been superimposed to indicate the temperature range for failure during Sigmajig testing. Note that cracking occurs within the brittle temperature range predicted by hot-ductility testing.

ductility is negligible and centerline cracking occurs. This assumes that essentially no microstructural modification occurs in the weld metal on-heating to the NDT. Using this approach, weld metal hot-ductility data and Sigmajig threshhold cracking results can be combined on a single diagram of fracture stress vs. temperature, as shown in Fig. 17.

This diagram shows that σ_{th} values lie within the BTR determined by hot-ductility testing and are biased to the low-temperature end of the BTR. This behavior is consistent with both the modified generalized theory for weld solidification cracking described by Matsuda, *et al.* (Ref.10), and the technological strength theory proposed by Prokhorov (Ref.11). These data are also consistent with recent experimental observations by Zacharia, *et al.* (Ref.12), who showed that cracking during Sigmajig testing occurs at some distance behind the trailing edge of the weld pool. Based on these observations and the fracture stress vs. temperature data in Fig. 17, it can be predicted that the temperature range in which cracking occurs during Sigmajig testing of A-286 is from approximately 1085° to 1140°C. This temperature range is within the BTR for A-286 predicted by Lin, *et al.* (Ref. 13), using the Varestraint test.

The fracture behavior of the Sigmajig and Gleeble hot-ductility specimens (for teardrop-shaped weld pools fractured above NST) are essentially identical, exhibiting the dendritic morphology illustrated in Fig. 9. These similarities, in conjunction with comparable fracture stresses as indicated above, demonstrate a reversibility of the cracking processes in this alloy. During solidification cracking, only a small proportion of eutectic liquid remains at grain boundaries and the stresses are sufficient to promote fracture. Alternatively, during liquation cracking these eutectic regions remelt and under the application of stress fracture in a similar manner. These results suggest that for weld metals that do not undergo significant microstructural modification during reheating, Gleeble hot-ductility testing can be used to predict the temperature range over which cracking occurs in the Sigmajig test.

Conclusions

1) Sigmajig testing determined that as the specimen yield strength increases the threshold stress for cracking (σ_{th}) decreases. The reduction in threshold stress is attributed to both strain localization and constraint factors at high temperatures that tend to increase local strain as a function of base metal yield strength.

2) A doubling of the Sigmajig sample thickness resulted in an increase in the threshold stress for cracking. This increase is attributed to constraint effects associated with the increase in specimen thickness.

3) Gleeble hot-ductility testing of weld metal specimens found that the brittle temperature range on-cooling is independent of the weld pool shape. The fracture location, however, is influenced by the weld pool shape, with the fracture of teardrop-shaped weld pool specimens occurring in the fusion zone above the NST and the fracture of elliptical-shaped weld pool specimens occurring exclusively in the HAZ.

4) The Sigmajig threshold stress data correlated well with fracture stress levels measured during Gleeble hot-ductility testing of specimens produced from a teardrop-shaped weld pool. Comparison of fracture stress and σ_{th} data indicated that failure during Sigmajig testing occurs in a narrow temperature range just above the ductility recovery temperature on-cooling.

5) Fracture surfaces of Sigmajig samples exhibited classic dendritic morphologies from the crack initiation point to where the crack arrested, with secondary dendrite arms less evident at the crack initiation location. These fracture morphologies were very comparable to those observed in Gleeble hot-ductility specimens which experienced fusion zone fracture.

Acknowledgments

The authors would like to express their appreciation to Rolled Alloys, Inc., for providing the A-286 stainless steel sheet material. We would also like to acknowledge valuable technical discussions with Dr. Gene Goodwin at operated by Lockheed Martin Energy Research Oak Ridge National Laboratory and Dr. Wangen Lin of Edison Welding Institute. This work was supported through the Cooperative Research Program at Edison Welding Institute.

References

1. Lippold, J. C., Harwig, D. E., Ernst, S. C., and Nelson, D. 1989. Development of a weldability test data base WELDTEST. Unpublished Research, Edison Welding Institute, Columbus, Ohio.
2. Goodwin, G. M. 1987. Development of a new hot cracking test, the Sigmajig. *Welding Journal* 66(2):33-s to 38-s.
3. Savage, W. F., and Lundin, C. D. 1965. The Varestraint test. *Welding Journal* 44(10):433-s to 442-s.
4. Goodwin, G. M. 1988. The effect of heat input and weld process on hot cracking in stainless steel. *Welding Journal* 67(4): 88-s to 95-s.
5. Unpublished research. Oak Ridge National Laboratory, Oak Ridge, Tenn.
6. Lin, W., Baeslack, W. A. III, and Lippold, J. C. 1991. A method for predicting HAZ liquation cracking using the Gleeble hot-ductility and spot-Varestraint tests. EWI Research Report MR91 11, Edison Welding Institute, Columbus, Ohio.
7. Chen, C. 1989. A comparative evaluation of solidification and liquation cracking in aluminum alloys. Ph.D. dissertation, The Ohio State University, Columbus, Ohio.
8. Lin, W., Lippold, J. C., and Baeslack, W. A. III. 1992. Analysis of weldability test techniques for HAZ liquation cracking. *Proc. of Third Int. SAMPE Metals Conference*, Toronto, Canada.
9. Lin, W., Lippold, J. C., and Baeslack, W. A. III. 1993. An investigation of heat-affected zone liquation cracking, part 1 — a methodology for quantification. *Welding Journal* 71(4): 135-s to 153-s.
10. Matsuda, F., Nakagawa, H., and Sorada, K. 1982. Dynamic observation of solidification and solidification cracking during welding with optical microscope. *Trans. JWRI* 11(2): 67–77
11. Prokhorov, N. N. 1971. Fundamentals for the theory of technological strength of metals while crystallizing during welding. *Trans. JWS* 2(2): 109–117.
12. Zacharia, T., *et al.* 1994. Dynamic stresses in weld metal hot cracking. *Welding Journal* 73(12): 164-s.
13. Lin, W., and Lippold, J. C. 1992. Weldability testing of austenitic stainless steels. *Proc. Eighth North American Welding Research Conference*, October 19–21, EWI, Columbus, Ohio.